Evaluation of a Novel Design for Emulating the Mechanical Behavior of Commercial Ankle Prostheses: A Redesign of the VSPA Foot

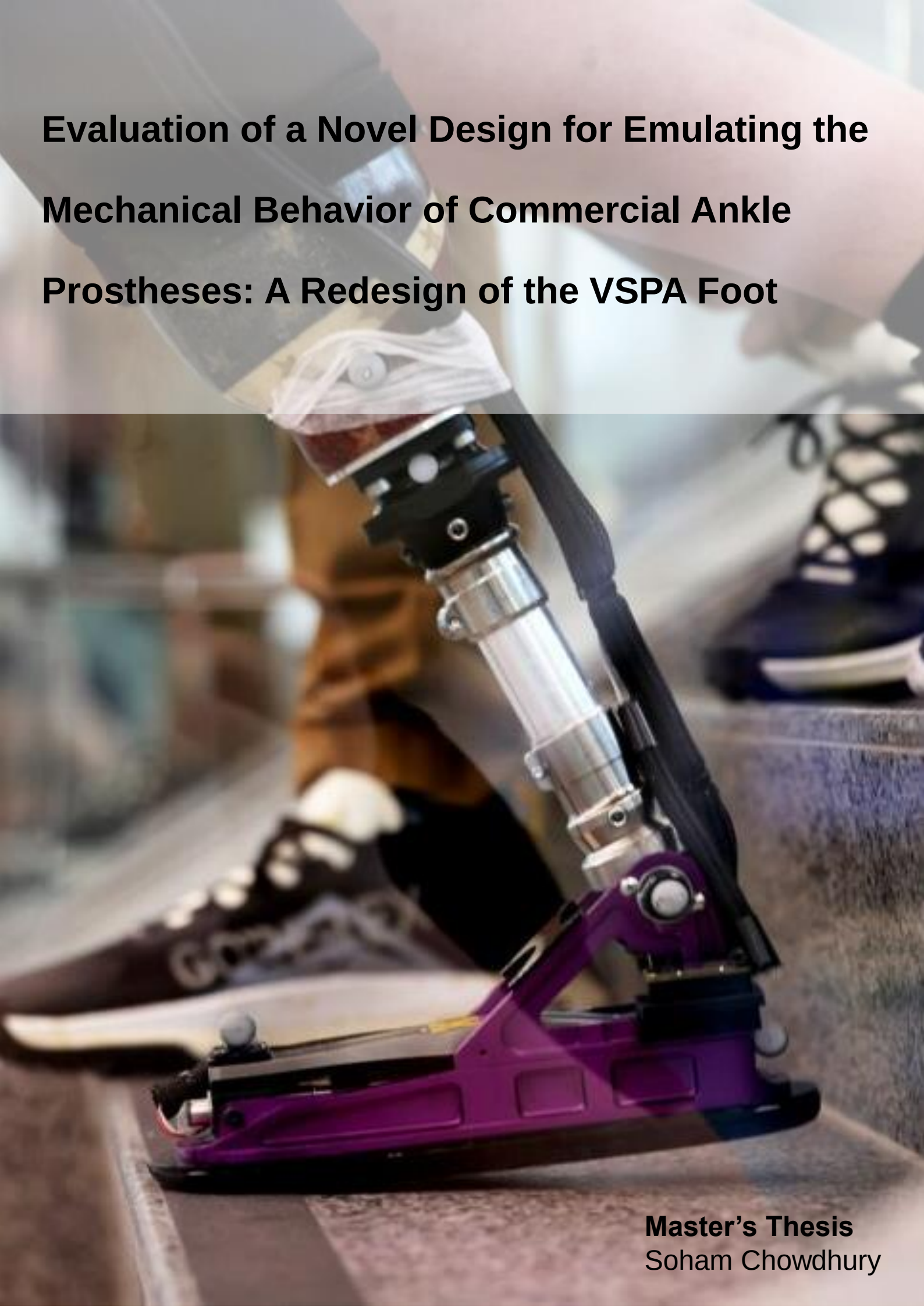

Master's Thesis

Soham Chowdhury

Evaluation of a Novel Design for Emulating the Mechanical Behavior of Commercial Ankle Prostheses: A Redesign of the VSPA Foot

by

Soham Chowdhury
(5726204)

Cover: Variable Stiffness Prosthetic Ankle by Neurobionics Lab University of Michigan (Modified)

Supervisors

MSc-Thesis Advisor:

- E.J Rouse PhD.
  ejrouse@umich.edu
  (734) 763-3629
  University of Michigan, Ann Arbor
  Department of Mechanical Engineering

- Dr.ir. G. Smit
  G.Smit@tudelft.nl
  +31 15 27 81688
  Delft University of Technology
  Department of BioMechanical Engineering

Professor:

- Prof.dr.ir. P. Breedveld
  P.Breedveld@tudelft.nl
  +31 15 27 85232
  Delft University of Technology
  Department of BioMechanical Engineering

Evaluation of a Novel Design for Emulating the Mechanical Behaviour of Commercial Ankle Prostheses: A Redesign of the VSPA Foot

Soham Chowdhury[a,b]

[a]*Neurobionics Lab, University of Michigan Ann Arbor, USA,*
[b]*Biomedical Engineering Department, Delft University of Technology, Delft, The Netherlands,*

Abstract

Background: Lower limb amputations significantly impact an individual's mobility and quality of life. Passive-elastic prosthetic feet are often prescribed to restore ambulatory functions; however, selecting the correct prosthesis for patients is challenging due to the diverse mechanical properties and designs of commercially available prostheses. Furthermore, prosthetic prescriptions rely heavily on clinical judgment rather than patient feedback. Current alternatives for prosthetic foot trials face logistical and practical limitations.
Objective: This study aims to develop and evaluate a novel ankle prosthesis emulator capable of emulating the mechanical behaviour of multiple commercial passive-elastic prosthetic feet, allowing for rapid back-to-back trials in both clinical and real-world environments.
Methods: The Variable Stiffness Prosthetic Ankle (VSPA) was modified to accommodate a multicam mechanism, allowing the emulation of five different prosthetic feet. Mechanical properties, such as the torque-angle relationship, were characterized for the emulated feet using finite element analysis (FEA) and mechanical testing with a 3D-printed prototype. The FEA predicted results and experimental results were compared with the original commercial prosthetic feet data to validate the emulator.
Results: The FEA predicted torque-angle relationship of the emulated prosthetic feet closely matched the mechanical properties of their corresponding commercial feet, with percentage errors of 2.87% in dorsiflexion and 9.28% in plantarflexion. The torque-angle relationship generated from the 3D-printed multicam mechanism exhibited a similar nature to the experimental data. However, the torque magnitudes were significantly less than the actual prostheses. The switching mechanism of the cam profiles was also successfully demonstrated by the 3D-printed setup.
Conclusion: Based on FEA the novel ankle prosthesis emulator can effectively replicate the mechanical behavior of commercial prosthetic feet, demonstrating its potential as a cost-effective and time-efficient tool for patient trials and prosthesis selection. However, the same needs to be validated based on real-world tests using the manufactured prototype. The 3D-printed multicam mechanism was not able to effectively emulate the commercial feet due to the dissimilarities in material properties of the 3D-printed and proposed components. Future work should focus on manufacturing the mechanism using the proposed materials and optimizing the structure to reduce weight and complexity for long-term clinical applications.

Keywords: Ankle prosthesis emulator, passive-elastic prosthesis, transtibial amputation, prosthetic foot prescription

1. Introduction

1.1. Background

The number of individuals with lower extremity amputations in the U.S. is projected to rise to 3.6 million by 2050, with major lower limb amputations expected to account for 38% of these cases [1]. Lower limb loss has a significant negative impact on physical function and psychosocial health, leading to a diminished quality of life. Following such a loss, lower limb prosthetic devices play a crucial role in rehabilitation, aiming to restore daily activities and enhance quality of life [2–4]. In this study, we focussed on the ankle prosthetic foot prescribed after transtibial amputation. Based on functionality and the level of supported activity, ankle prostheses can be broadly categorised as passive, quasi-passive, and active/powered prostheses [5]. Comparing the different prosthetic devices we found that although powered prosthesis allows a more biomimetic gait, it does not significantly improve other biomechanical factors such as reducing metabolic cost, improving balance etc (Appendix). Thus passive prostheses are often preferred because they are relatively cheap, lightweight and allow individuals to perform daily ambulation tasks [6]. However, choosing the correct passive prosthesis is crucial as this impacts tasks such as foot positioning, walking on flat surfaces, navigating ramps and stairs, crossing obstacles, walking on slippery surfaces, and transitioning between activities [7, 8].

Thus when prescribing a prosthesis, prosthetists and clinicians must consider several factors such as the type of prosthesis, the degree of prosthetic integration/ familiarisation, the level and cause of amputation, the individual's mobility, the desired functional level and the presence of comorbidities [9–11]. Furthermore, the overwhelming number of prostheses with varying mechanical properties, overall construction, and cost make the appropriate pairing of a prosthesis with an am-

putee end user more complicated [12, 13]. Presently, decision-making during the prosthetic foot prescription is skewed significantly by the clinicians' judgement over patient involvement. Patients are often unaware of the potential options available. Moreover, very few patients can participate in experimental trials evaluating the functional performance of different feet and provide input regarding prosthesis features that can positively affect their desired ambulation tasks. This results in the absence of patient feedback in the decision-making process [10, 14, 15]. Review studies also show that the available scientific evidence is inadequate to establish a universal prosthesis prescription protocol to compare multiple commercially available passive-elastic prosthetic feet [16].

1.2. Alternative Approaches to Regulate Prosthetic Foot Prescription

One method to incorporate patient preferences into the selection of prosthetic feet is to enable patients to trial various options [17]. Currently, clinicians could acquire multiple prosthetic feet and allow patients to test each one briefly, returning those that are not chosen. However, this approach poses significant challenges, including the logistical burden of managing a large inventory and the need for frequent prosthetic adjustments due to varying build heights among feet. Additionally, it does not facilitate immediate, direct comparisons between feet. Another strategy involves using a robotic prosthetic foot emulator to replicate the mechanical properties of different commercial feet (Figure 1)[18–20]. While this method allows for controlled comparisons, it is also limited by factors such as the high cost of the system and the restriction of testing to clinical or laboratory settings.

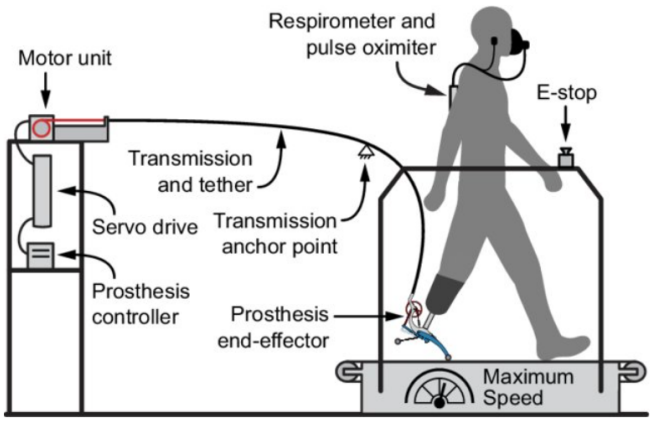

Figure 1: The robotic ankle prosthesis emulator consists of a lightweight end effector worn by the user actuated by a flexible tether attached to a motor and a control system. The motor can be programmed to exert the desired ankle moment for emulating the chosen ankle prosthesis. *Adapted from [21]*

As an innovative alternative, a novel ankle prosthesis emulator has been proposed in this study. This emulator builds on the foundational Variable Stiffness Prosthetic Ankle (VSPA) originally developed by Shepherd and Rouse (2017), which has been modified to incorporate five interchangeable cam profiles [22]. Each cam profile is encoded with the specific mechanical characteristics of commonly prescribed commercial passive-elastic ankle prosthetic feet. Through these encoded profiles, the emulator is designed to replicate the ankle torque-angle relationship of various prosthetic foot models along with their designated manufacturer stiffness categories. This capability is achieved by incorporating a rotating cam mechanism that facilitates rapid, back-to-back evaluation of multiple prosthetic feet in realistic, clinical, or laboratory environments.

This emulator approach eliminates the need for time-consuming adjustments that are typically required when switching between different physical prosthetic feet. Traditionally, each switch necessitates altering hardware such as the prosthesis length to accommodate differences in build height, as well as recalibrating the alignment and securing pylon components for each foot type. Such a manual exchange often proves labour-intensive and involves iterative adjustments by trained clinicians or technicians, which can substantially prolong the assessment process. In contrast, the proposed ankle prosthesis allows for the user's leg length and static alignment to be set once. This fixed configuration enables the prosthetist to prioritize fine-tuning dynamic alignment adjustments for each emulated foot, rather than reconfiguring fundamental setup elements [23, 24]. This streamlined process not only improves efficiency but also supports a faster transition between different foot models, potentially enhancing clinical workflows and patient experience. The capacity to easily switch between cam profiles within a single emulator facilitates a quicker and more efficient method for exploring a range of stiffness and mechanical behaviours in one session, providing immediate feedback for optimizing prosthetic alignment and functionality.

In designing this emulator, the replication of the mechanical properties of commercial prosthetic feet was prioritized, with a particular emphasis on accurately reproducing each foot's characteristic ankle torque-angle relationship. The torque-angle relationship, which reflects the interaction between applied torque at the ankle and the corresponding angle of rotation, has been demonstrated to significantly influence user preference and metabolic energy expenditure. The torque-angle characteristic of a passive-elastic foot is guided by the material properties and geometry of the foot [25, 26]. Therefore, emulating this relationship has the potential to provide users with an experience that more closely resembles their chosen prosthetic foot's biomechanical characteristics.

The current study's approach to accurately capture and emulate the torque-angle relationship involved conducting mechanical testing on each prosthetic foot to determine the torque output at specified ankle angles. This approach was selected as a direct and precise method to assess the distinct mechanical behaviors associated with each prosthetic foot. The use of mechanical testing provides a reliable data set from which the torque-angle curve can be derived, thus enabling each cam profile within the emulator to be precisely tailored to replicate the specific dynamics of the original prosthetic foot. Through this method, an objective characterization of the ankle torque-angle relationship has been achieved, facilitating a closer approximation of each foot's behaviour within the emulator. This novel

approach holds promise for enhancing the functionality of prosthetic testing protocols by providing a rapid, flexible, and accurate tool for clinical evaluations.

1.3. Research Goals

This study aimed to establish the feasibility of using our novel ankle prosthesis for rapid emulation of multiple commercial passive-elastic prosthetic feet using a combination of Finite Element Analysis and mechanical testing of a 3D printed setup. The secondary aim is to set up a database with objective metrics from characterising the five common clinically prescribed commercial prosthetic feet. This database can also aid in comparing prosthetic feet for prescribing prosthetic feet.

2. Design

2.1. VSPA Design Description

The VSPA foot design, originally developed by Shepherd and Rouse (2017), serves as the primary component in the proposed mechanism. The cam transmission system of the original VSPA foot was redesigned to accommodate multiple cams and to emulate various passive elastic prostheses [22]. Originally, the VSPA foot, a quasi-passive prosthetic device, successfully replicated biological torque-angle curves at the ankle joint through a cam-based transmission system combined with a variable stiffness cantilever spring (Figure 2). These torque-angle curves were derived from kinetics and kinematics data collected for activities such as normal walking, stair climbing, and descent, thereby referencing the capabilities of able-bodied ankle joints [27]. Biological ankle joints perform net positive work during the push-off phase in the normal walking gait cycle. The push-off phase (stage 4 in Figure 3) cannot be replicated by a quasi-passive prosthesis, as it does not generate energy. Here, 'quasi' indicates the presence of an actuator within the prosthesis, which alters its properties without injecting energy into the gait cycle [28]. In the absence of energy generation, the VSPA foot mimics human ankle behavior during the "controlled plantar flexion" and "controlled dorsiflexion" phases, achieved through a non-linear spring system.

The cam transmission system includes a cam profile and follower that mechanically link the prosthetic ankle joint to a cantilever spring. Desired torque-angle curves are produced by adjusting the cam profile's shape, which, along with ankle joint rotation, governs the downward deflection of the spring and the elastic energy it stores. The normal contact force between the cam profile and follower is determined by spring deflection and, by design, remains independent of the weight of the VSPA foot wearer.

The primary torque-angle curve of the VSPA foot is determined by the cam profile's shape, while overall stiffness can be modified by altering the cantilever spring's effective length. Adjustments to the simple support point on the spring are made by translating it along a lead screw with a small motor. This repositioning is performed during the swing phase, when the foot is off the ground, allowing the cam follower to travel to the equilibrium point of the cam profile. At this point, the normal contact force between the cam and follower becomes equivalent to the minimal preload, preventing motor overloading and energy injection into the walking cycle. The capacity for modifying spring stiffness facilitates customization of the torque-angle curve to suit user comfort and specific ambulatory tasks.

2.2. Design Requirements

2.2.1. Functional Requirements

Functional requirements define the essential parameters the proposed design must meet, guiding the design process and establishing boundary conditions for evaluating functionality, manufacturability, and assembly. This study aims to develop and validate an emulator design based on the VSPA foot that replicates the mechanical behavior of commercial passive-elastic prosthetic feet, enabling rapid testing of emulated prostheses. Here, the ankle torque-angle relationship characterizes prosthesis mechanics, necessitating minimal differences between experimental torque-angle data from actual and emulated prostheses. Multiple cam profiles encoded with the mechanical properties of passive-elastic prosthetic feet are used to achieve this goal. To facilitate the maximum number of back-to-back demonstable prosthetic feet the cam housing should be designed to accommodate the corresponding number of cam profiles.

The VSPA foot's existing feature for altering the overall stiffness of the torque-angle curve by adjusting the slider (simple support) with a motor and lead screw is retained, though stiffness variability is not a central feature of the multicam mechanism. Stiffness variability may be useful for assessing patient preferences in prosthetic ankle stiffness while testing emulated passive-elastic feet. Excess mass in the VSPA multicam foot would raise metabolic costs during normal gait, and substantial weight differences between a user's prosthetic foot and the emulator may result in compensatory gait strategies, preventing an objective comparison across different emulated prostheses. Therefore, the system's overall mass must be minimized.

The emulator's range of motion (ROM) should align with that of the human ankle joint. The ankle joint ROM during normal walking gait spans 20° in plantarflexion and 12° in dorsiflexion. Passive-elastic prosthetic feet, which do not produce net positive work during the gait cycle, exhibit a reduced plantarflexion ROM of approximately 5°. The distance between the ankle rotation axis and the cam profile's equilibrium point influences the torque in the VSPA foot and must remain consistent with the original design to preserve the mathematical integrity of the cam profile geometry. To enable efficient back-to-back trials of emulated feet, a mechanism for quick and manual cam switching is required. The functional criteria guiding this study are outlined in Table 1.

2.2.2. General Requirements

Material selection for manufacturing must ensure that the device resists plastic deformation under the high dorsiflexion and plantarflexion loads. Customization is necessary to allow testing of emulated prostheses with varied stiffness, size, and function. The design should support modularity, allowing cam pro-

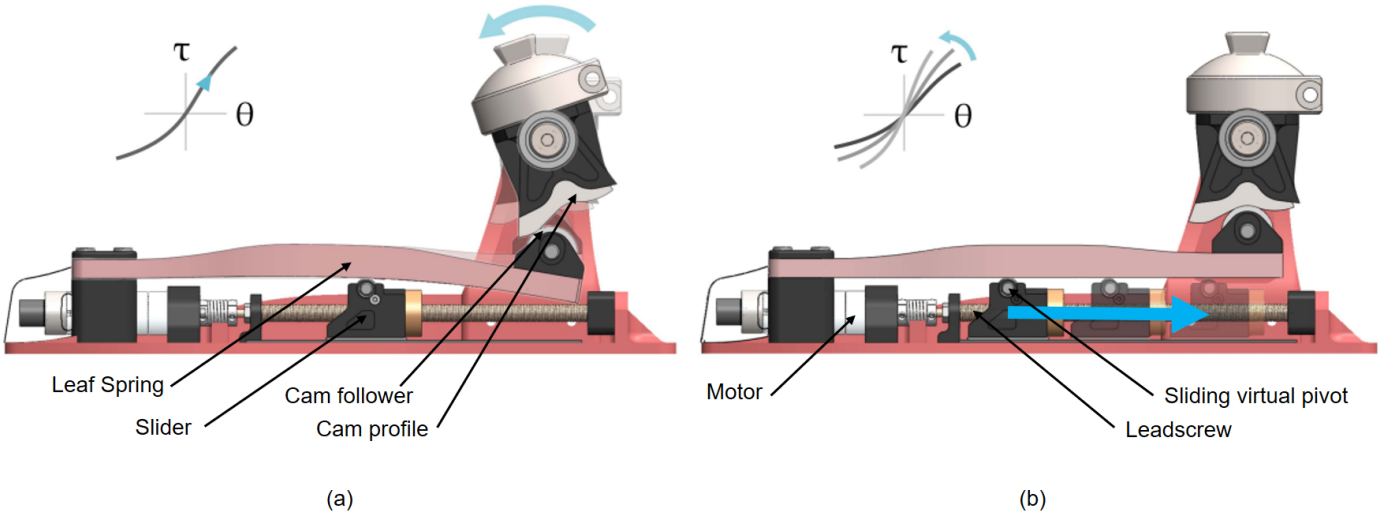

Figure 2: Design elements in the VSPA foot for generating a non-linear torque angle curve and modulating its overall stiffness: (a) The cantilever spring deflects downward due to the cam profile pushing the cam follower; exerting a reaction torque at the ankle joint as the joint rotates. The shape of the cam profile enables the VSPA foot to produce non-linear torque angle curves. (b) A leadscrew attached to the motor controls the slider (simple support) position. The primary torque-angle curve is generated when the slider is at the mid-point (primary position) of its range of motion. Changing the slider position changes the overall stiffness of the torque-angle curve. *Adapted from [22].*

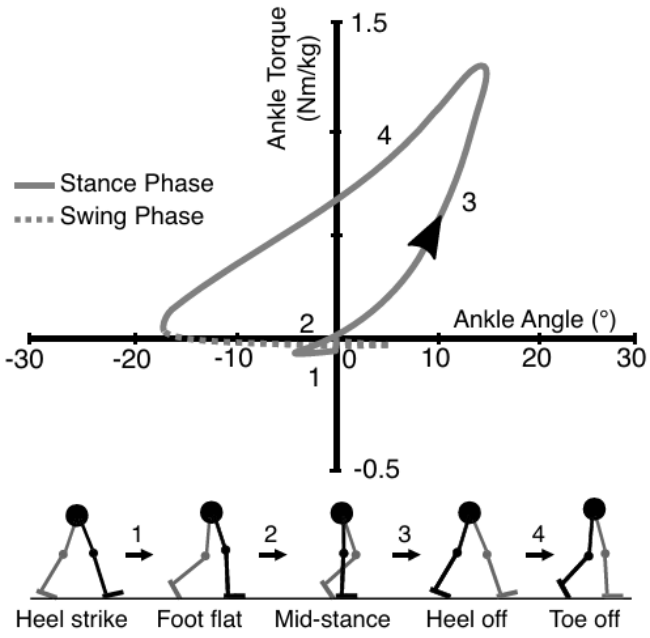

Figure 3: The torque generated by the ankle of an able-bodied subject when performing normal walking gait is plotted against the ankle angle. The four main stages of the stance phase are depicted below the torque-angle curve. The push-off phase indicated by '4' during the gait cycle represents positive work done by the ankle and thus can't replicated by the passive prosthesis. *Adapted from [29].*

files to be swapped with minimal component changes. Additionally, ease of dis(assembly) should be prioritized to enhance reproducibility, independent of clinician involvement. To minimize design costs and complexity, the use of off-the-shelf components and the exclusion of bushings and bearings is preferred.

2.3. Previous Design Iterations of the Multicam Mechanism

2.3.1. Sliding Cam Mechanism

A sliding cam mechanism was devised to facilitate switching between cam profiles that are encoded with the specific torque-angle characteristics of commercial passive-elastic prostheses, as depicted in Figure 4. In this mechanism, the cam profiles are aligned parallel to the sagittal plane within a slotted housing, thus allowing mediolateral sliding to occur. Electromagnets placed on either side of the frame govern the sliding motion by applying directional control, while a ridge embedded within the frame restricts movement to the mediolateral axis, effectively eliminating other degrees of freedom. As shown in Figure 4, this configuration employs a three-cam setup. To enable sequential engagement across these three cams, the mechanism is designed with five empty slots that allow for precise cam positioning. When both electromagnets are activated, the cam cluster is directed to the center, thereby engaging the middle cam profile. By alternating the activation of electromagnets, the cam follower can selectively engage either the cam to the left or right of the middle cam, depending on which electromagnet is triggered. Cam switching is optimized to occur when the ankle angle reaches zero—specifically, when the follower is positioned at the equilibrium point of the cam profile. This approach minimizes frictional forces by reducing the normal force between the cam and the follower at the equilibrium position, enabling smooth mediolateral sliding.

This design offers the advantage of very low transition times for a three-cam setup, which is particularly beneficial in applications where rapid transitions are essential. However, the mechanism's optimal loading capacity remains limited to three cams. Expanding the number of cams introduces complexity in position control and necessitates additional actuation mechanisms, which could impair the system's overall efficiency and usability. This limitation restricts the capability for rapid, back-

Table 1: Overview of the Design Requirements

Criteria	Parameter	Requirement
Functional	Emulating the passive-elastic prostheses	Within <5% estimation of torque-angle curves of the prostheses with the VSPA multicam foot.
	Number of cam profiles	Number of cams > 3
	Quasi-passive	Maintain stiffness variability feature of the VSPA foot
	Mass	Overall weight of the multicam subassembly and the VSPA foot should not exceed 1.5kg
	Range of Motion	Range of Motion of the emulator: >20° in plantarflexion and >15° in dorsiflexion
	Dimentional constraint	Distance from the ankle axis to the equilibrium point = 43.5mm
	Transition time	Transition time between two sequential cams should be <2s
General	Customisability	The mechanism should accommodate emulated prosthetic feet from different stiffness categories, sizes and functional support
	Modularity	The mechanism should be easily (dis)assembled
	Off-the-shelf components	Off-the-shelf components should be used to lower the cost

to-back testing of more than three prosthetic feet, which may be required for comprehensive comparative studies. Furthermore, the sliding action between cam profiles and the cam follower generates high frictional forces during transitions, accelerating wear on the cam profiles over time. Increasing the cam quantity would also necessitate a wider frame to accommodate additional profiles, requiring a larger VSPA foot assembly and subsequently increasing the overall weight of the prosthetic ankle. This added weight could impose an additional metabolic cost for users and could compromise the device's performance in clinical and daily life applications.

2.3.2. Rotary Disk Mechanism

To address the spatial and operational constraints observed in the sliding cam mechanism, a rotary disk mechanism was developed. This design arranges cam profile pairs radially on a rotating disk with a central shared region, as shown in Figure 5. The rotation axis of the cam disk is approximately perpendicular to the transverse plane, enabling a rotational motion that differentiates it from the linear mediolateral sliding mechanism of the previous design. The circular section at the disk's center acts as a common engagement region for the torque-angle relationship, positioned close to the equilibrium point (ankle angle zero) for all cam profiles. Around this central area, distinct dynamic cam segments are situated and inserted into designated slots on the cam disc. Together, the central static cam region and the dynamic cams form a complete cam profile that emulates the dorsiflexion and plantarflexion cycles. The central static cam region is equipped with a ridge that restricts rotation to the transverse plane, effectively removing all extraneous degrees of freedom. When the cam follower is positioned within this shared region, the dynamic cam profiles are disengaged, permitting manual rotation of the disk to select alternative cam profiles. Additionally, this mechanism allows for unique combinations of dorsiflexion and plantarflexion cam profiles by positioning dynamic cams on opposite sides of the disk, further expanding its versatility.

A significant advantage of the rotary disk design is its ability to considerably reduce wear on cam profiles during switching. When the cam follower is engaged with the central static

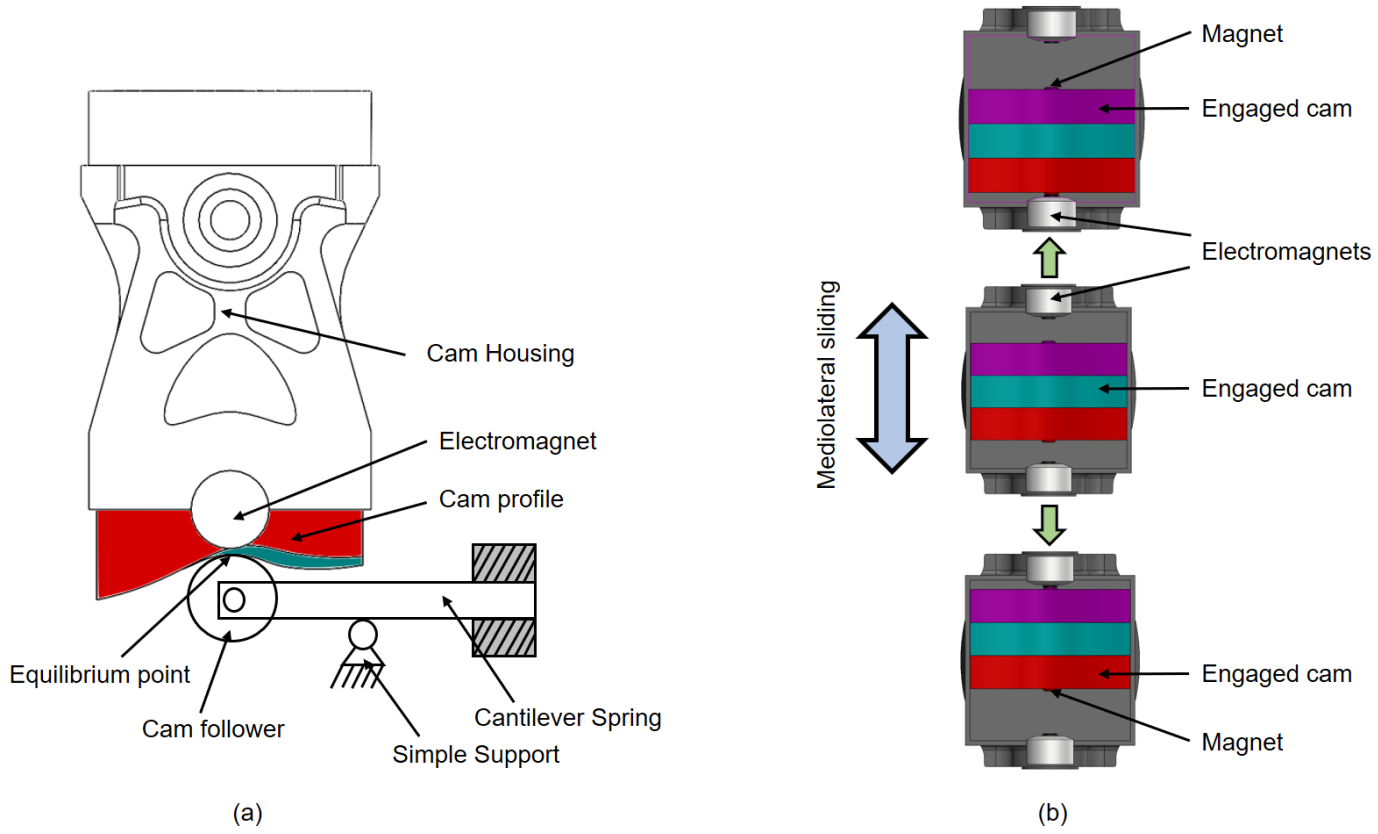

Figure 4: Sliding cam mechanism: (a) The cam follower is at the equilibrium point of the cam profile when the angle at the ankle is zero. (b) At this cam follower position, the cam profiles can be switched by sliding mediolaterally in the groove at the base of the cam housing. The three cams are color-coded to identify the engaged cam. The position of the three-cam cluster is controlled using the electromagnets located at either side of the cam housing base. Magnets are provided on the surface of the cams that flank the middle cam to lower the transition time. Three positions of the cluster are shown where each cam gets sequentially engaged with the cam follower.

cam, no high frictional forces act upon the surrounding dynamic cams, resulting in a reduced rate of wear and longer operational lifespan for each profile. However, the design is constrained by spatial limitations; the VSPA frame must be widened to structurally support the disk. This necessity increases both the weight and size of the prosthetic ankle, which could limit the mechanism's applicability for lightweight prosthetic designs or users with specific mobility requirements. Moreover, the addition of extra cam profiles can only be achieved by narrowing the width of each cam profile, which in turn increases stress concentration in areas subjected to high normal forces by the cam follower. This could compromise the structural integrity of the profiles and diminish the device's durability over extended use.

2.3.3. Rotary Barrell Mechanism

In response to the spatial limitations of prior designs, a rotary barrel mechanism was proposed as an alternative. This mechanism arranges the cam profiles around a barrel that is rotated via a barrel pin, as illustrated in Figure 6. In this configuration, the rotation axis of the cam barrel aligns perpendicular to the frontal plane when the ankle angle is zero. Distinct from previous designs, this configuration does not incorporate a stationary shared central region. Instead, an uninterrupted cam profile construction is provided, enhancing the seamless continuity between different cam profiles. Additional customization of cam positioning is achievable by sliding the individual cams along the barrel. Switching between cams is designed to occur when the cam follower is at the equilibrium point of the cam profile, a feature that minimizes frictional forces and reduces wear during transitions. The rotary barrel is capable of housing up to five cam profiles, allowing for the sequential testing of five emulated prosthetic feet without necessitating frequent reassembly. However, adding more cam profiles would require modifications to the structural support of the main housing frame, as additional cams would decrease the area available for the necessary support structures.

The rotary barrel design is notable for its absence of a shared region in the cam profile, which enhances the accuracy in replicating the passive-elastic mechanical behavior of commercial prosthetic feet. This continuous design approach facilitates a more precise emulation of the ankle joint mechanics, but also introduces a potential drawback: significant frictional forces develop between the cam profile and follower during profile switching, which increases wear on the cam surfaces and may hinder the ease of rotation. Additionally, the high normal forces acting on the barrel could make cam rotation challenging and

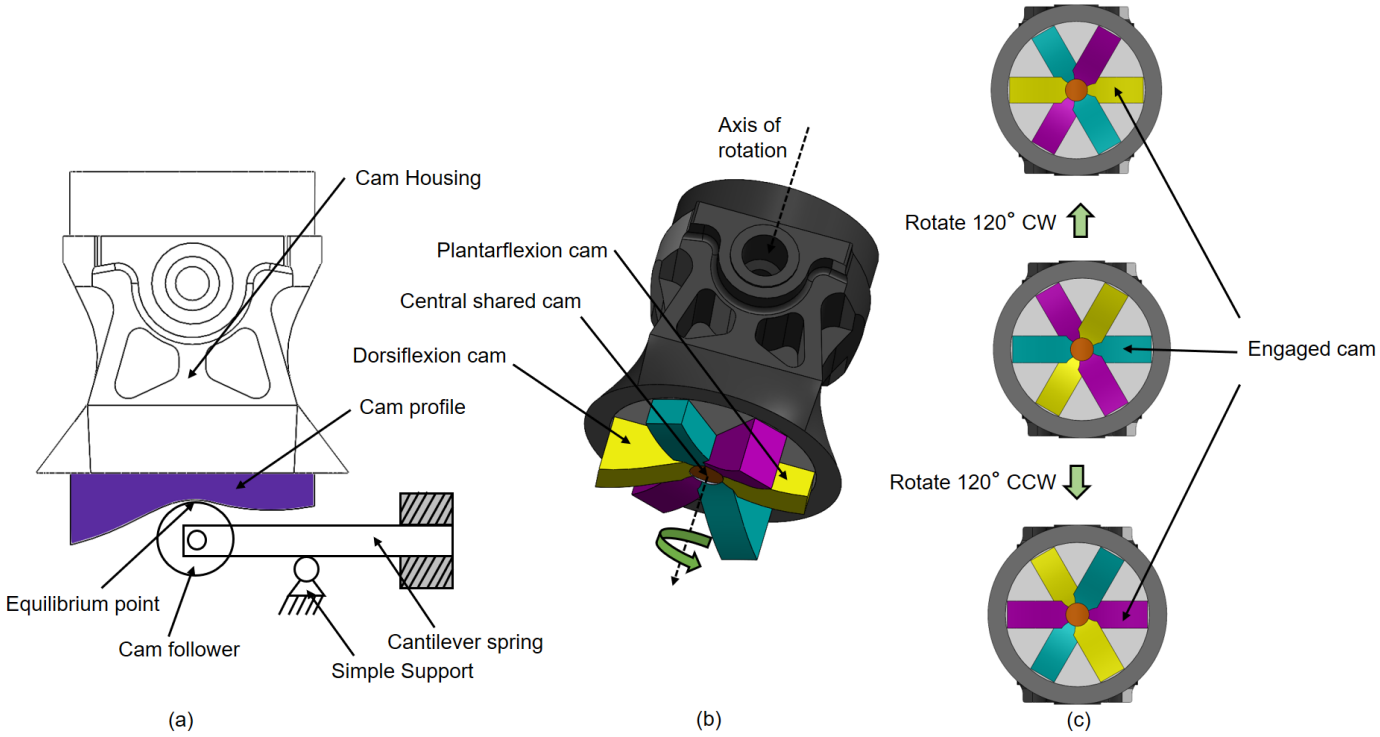

Figure 5: Disc cam mechanism: (a) The cam follower is at the equilibrium point of the cam profile when the angle at the ankle is zero. In this view, the two other cam profiles are hidden to ease understanding. (b) At this cam follower position, the cam profiles can be switched by rotating the dynamic cam hub about the axis passing through the centre of the shared static cam. (c) The cams get sequentially engaged with the cam follower as the dynamic cam hub is rotated. The cams are color-coded to identify the engaged cam.

necessitate increased torque for smooth operation. The lack of central support structures introduces a potential risk for barrel shaft buckling, especially when emulating very stiff prosthetic feet that require higher resistance. Unlike other designs, this rotary barrel configuration does not support independent customization of the dorsiflexion and plantarflexion torque-angle behaviors, limiting its adaptability to variations in user gait patterns or individual prosthetic requirements.

2.4. VSPA Multicam Design Description

The proposed design (Figure 7) preserves the VSPA foot's cam-based transmission. While only the primary torque-angle curve is used, motorized support was positioned at the midpoint of its motion range, allowing spring stiffness modulation based on participant comfort during clinical trials.

To emulate the mechanical behavior of commercial prosthetic feet, five passive ankle prostheses were characterized, and torque-angle curves were determined for their respective ankle ROM. The torque-angle and cam profile geometry relationship, initially developed by Shepherd and Rouse (2017), was applied to generate the cam profiles [22]. The full mathematical algorithm is detailed in the Appendix.

The cam profiles were divided into three sections namely, the dorsiflexion curve, central shared curve and plantarflexion curve. The central curve spans 5mm in length (corresponds to a range of motion ±2.3°) and is shared by all the cam profiles. The geometry of the central curve was determined by averaging the curve within the coordinates ±2.5 mm from the equilibrium point for all the determined cam profiles. The dorsiflexion and plantarflexion curves as their names suggest correspond to the dorsiflexion and plantarflexion loading of the ankle prostheses respectively. Similarly, the rotary hubs for mounting the cam profiles were divided into a dorsiflexion hub and a plantarflexion hub. Both the rotary hubs were attached to the main housing using a pentagonal shaft. The cam profiles are fitted into their corresponding hubs to switch between the emulated commercial prostheses. At a time, five cam profiles can be mounted by sliding them into the provided slots in the hub. The slotted design allows easy dismount and swaping of the different cams. Switching between the cams is done when the cam follower is at the equilibrium position of the cam profile. Since at the equilibrium position, the cam follower is only in contact with the central shared cam, this helps in easy rotation of the cam barrels and prevents wear. The hub is rotated with a hex key by fitting it into the shaft head's hexagonal recess. To prevent accidental rotation of the hub, a retractable spring plunger was used to fix the hub after the desired cam profile was selected. Along with reducing the wear on the cam profiles when rotating the hub, this design also facilitates the incorporation of dorsiflexion and plantarflexion behaviours from different prosthetic feet. The ankle range of motion was extended from the respective commercial prosthetic ankles to be adjusted between 40°in dorsiflexion and plantarflexion. To minimize weight and complexity, the use of bushings and bearings was omitted during the

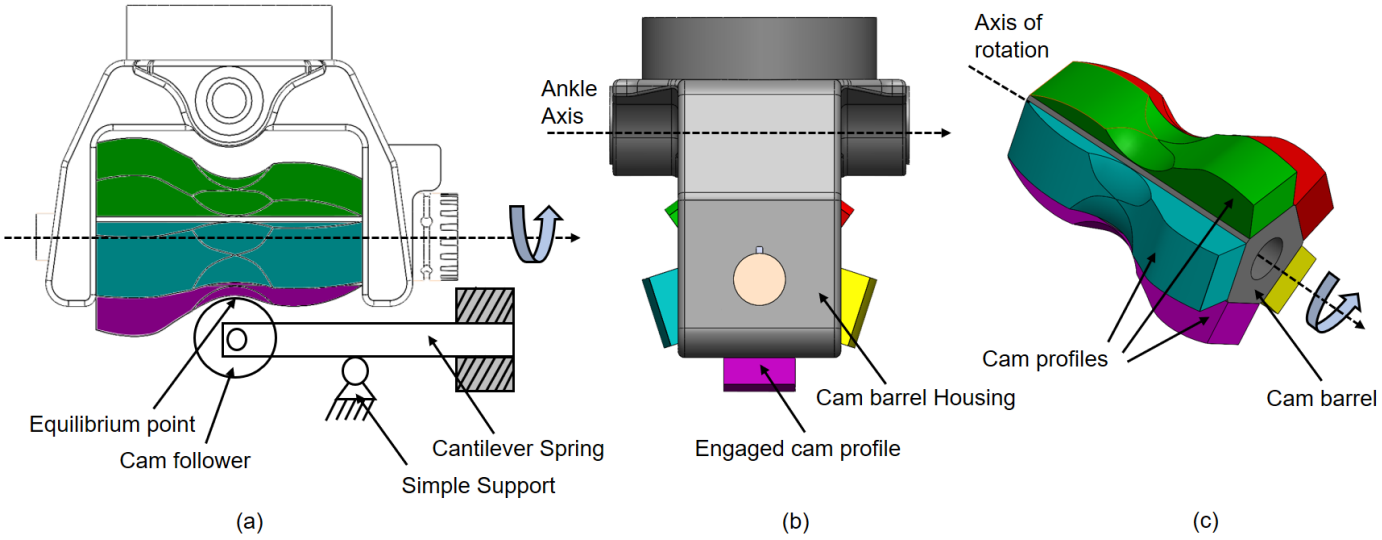

Figure 6: Rotary barrel cam mechanism: (a) The cam follower is at the equilibrium point of the cam profile when the angle at the ankle is zero. (b) At this position, the cam follower the cam profiles can be switched by rotating the cam barrel about the axis passing through the centre of the shared common cam profile. (c) The cam barrel where the five color-coded cam profiles are attached. The colors will help to identify the engaged cam

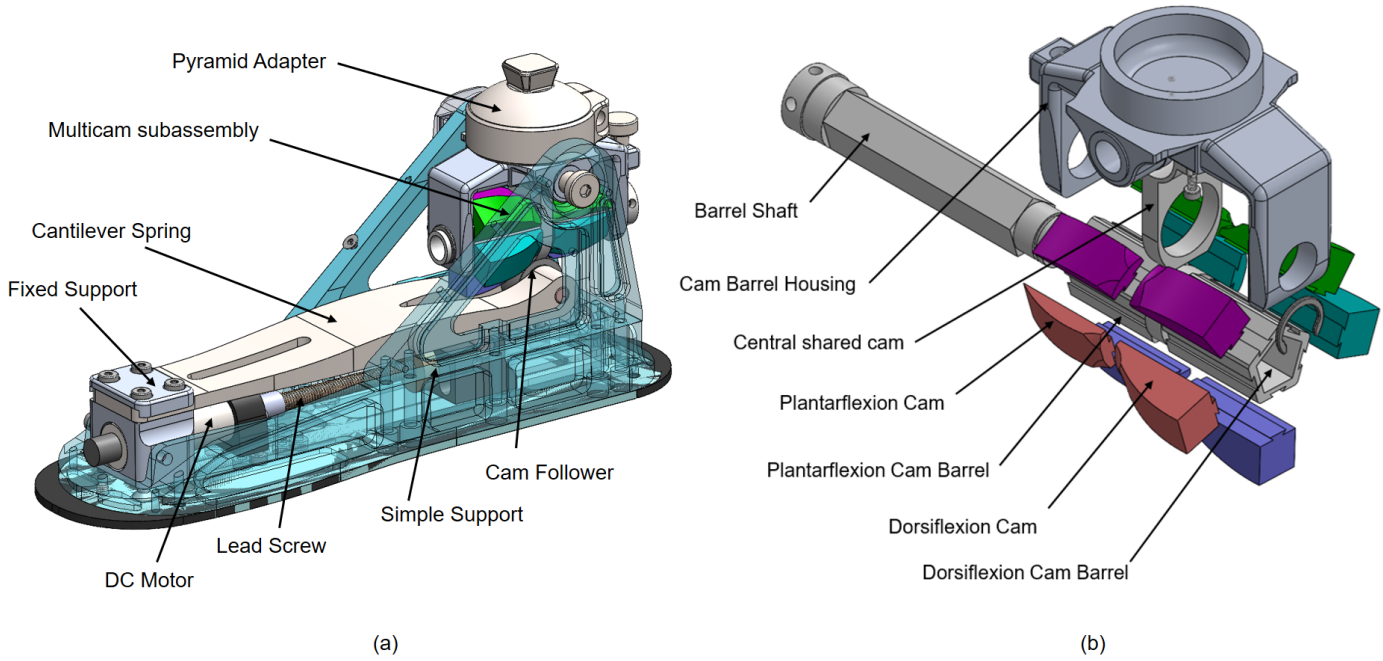

Figure 7: VSPA foot with the multicam subassembly: (a) Rotation at the ankle joint will deflect the cantilever spring providing a reaction torque at the ankle joint. This is the primary torque-angle characteristic of the engaged cam profile. By using the motor located at the forefoot the slider position can be altered, changing the overall stiffness of the primary torque-angle curves for each cam profile. (b) Exploded view of the multicam subassembly illustrating the designed components. The dorsiflexion and plantarflexion cams can be slid on and off the slots provided in their corresponding cam barrels. The barrel pin is secured to the housing by a C-clip. Accidental rotation of the barrel is prevented using the spring plunger.

assembly of components.

Tolerances were carefully defined to minimize clearances, preventing unwanted movement of the assembled components while ensuring sufficient space to allow smooth rotation of the cam barrels. For the component pairs which are intended to have relative motion, a H7/g6 tolerance was used. For the static components, H7/h6 tolerance was used. Given that the cams bear loads up to 7 kN, they will be machined from A8 air-hardened tool steel, chosen for its exceptional toughness and wear resistance. The cam housing/frame will be machined from 7075 Aluminum due to its high strength-to-weight ratio. Wire EDM will be selected as the machining process to achieve the highest accuracy in cam profile geometry. The cams will be hardened to Rockwell C 60 to prevent plastic deformation under

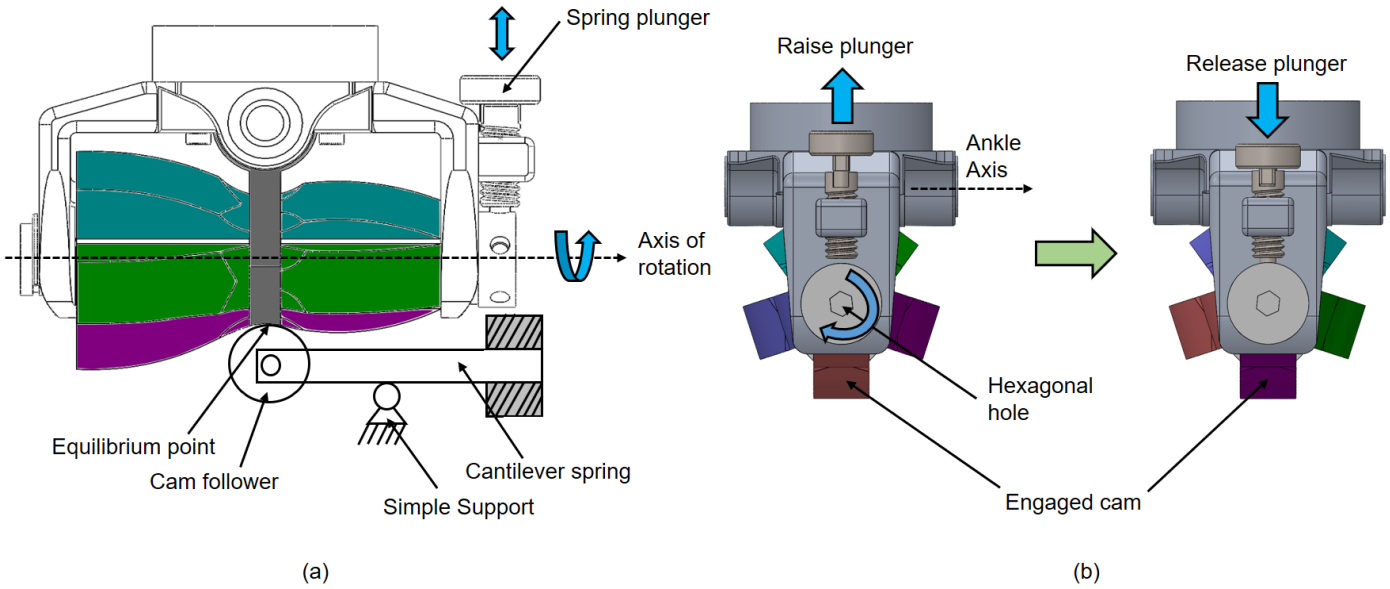

Figure 8: Rotating multicam mechanism: (a) The cam follower is at the equilibrium position of the cam profile when the angle at the ankle joint is zero. (b) Illustration of the steps to switch the cam profiles when the cam follower is at the equilibrium position. First, the spring plunger is raised to allow rotation of the cam barrel. Then the barrel is rotated by inserting a hex key in the hexagonal recess until the desired cam profile is reached. The spring plunger is then released securing the barrel position. The cam profiles are colour-coded to identify which prosthetic feet are being emulated.

high compressive contact forces. Hardening will be performed prior to machining to avoid any distortion of the cam geometry post-hardening.

3. Methods

Five clinically prescribed commercial passive-elastic prosthetic feet were characterized to estimate their respective torque-angle curves, as outlined in Table 2. For consistency across tests, all prosthetic feet were standardized to a size 26. Additionally, different stiffness categories were characterized for certain feet to evaluate whether alterations in cam profile geometry would be required or if modulation of spring stiffness alone would suffice. The observed mechanical behaviours of these prosthetic feet were subsequently used to establish a reference base for the target torque-angle curves.

The torque-angle curves were obtained using the Neurobionics Lab Rotary Dynamometer, a custom-built device equipped with a six-axis load cell (45E15AM63J, JR3, Inc., Woodland, CA, USA) mounted inline with a motor (BSM90N-3150AF, Baldor, Fort Smith, AR). The specified ankle range of motion was provided by the user, with torque output data sampled at 1000 Hz. During testing, the base of each prosthetic foot was securely mounted on a loading platform, which was then attached to the motor. For high-profile prostheses (those with a build height exceeding 70 mm from heel to pyramid adapter [30]), the pyramid adapter was attached directly to a jig (illustrated in Figure 9) while keeping the top fixed. In the case of low-profile feet (build height under 70 mm), a pylon was affixed to the pyramid adapter before securing it to the jig. The consistent positioning of the ankle axis across all prostheses was ensured by positioning the loading platform and the use of pylons in low-profile feet. To prevent shear movement between the prosthesis and platform, a 1/8" Delrin acetal resin sheet was utilized, thus minimizing the risk of system overconstraint [31]. All prosthetic feet were donned with their corresponding spectra sock and foot shell; however, shoes were excluded to isolate the mechanical properties of the feet alone. This approach ensured that the emulated mechanical properties would remain unaffected by shoe selection, thereby accommodating individual patient preferences [32]. Each prosthetic foot was preloaded with a force of 4–6 N to prevent any loss of contact with the platform throughout testing. The torque-angle curves were generated using each foot's specified range of motion. The loading and unloading process was automated using a custom MATLAB script (MathWorks Inc., Natick, MA, USA), wherein the maximum dorsiflexion and plantarflexion angles were inputted, and the platform applied a uniaxial torsion load by rotating about the ankle axis. The reaction torque exerted by each prosthesis was measured via the inline load cell. To replicate a quasi-static loading and unloading cycle for dorsiflexion and plantarflexion, the platform rotated at a constant rate, calculated as the maximum input angle divided by a preset time of 120 seconds. Platform angles were recorded using a motor encoder in conjunction with EPOS Studio software (Maxon Motor). Each prosthetic foot underwent three consecutive loading-unloading cycles, which were then averaged to determine the final torque-angle curves.

3.1. Data Analysis and Cam Profile Generation

The torque-angle data obtained for each prosthetic foot were filtered using three tenth-order notch filters, spaced at 30 Hz increments and with an 8 Hz bandwidth. A second-order But-

Table 2: Specifications of all the tested passive-elastic prosthetic feet

Manufacturer	**Prosthesis Model**	**Stiffness Category**	**Optimal Range of Motion**	**Maximum Supported Bodyweight (kg)**
Fillauer, Inc.; Chattanooga, TN	All Pro 	B4	± 15°	72.1
		C5	± 15°	90.3
		D6	± 15°	112.9
Össur; Reykjavik, Iceland	Variflex 	5	± 15°	88
Trulife; Detroit, MI	Seattle Lightfoot 2 	7	± 10°	86.2
Össur; Reykjavik, Iceland	K2 Sensation 	2	± 15°	80
		3	± 15°	97
		4	± 15°	114
College Park; Warren, MI	Trustep 	6	± 15°	91

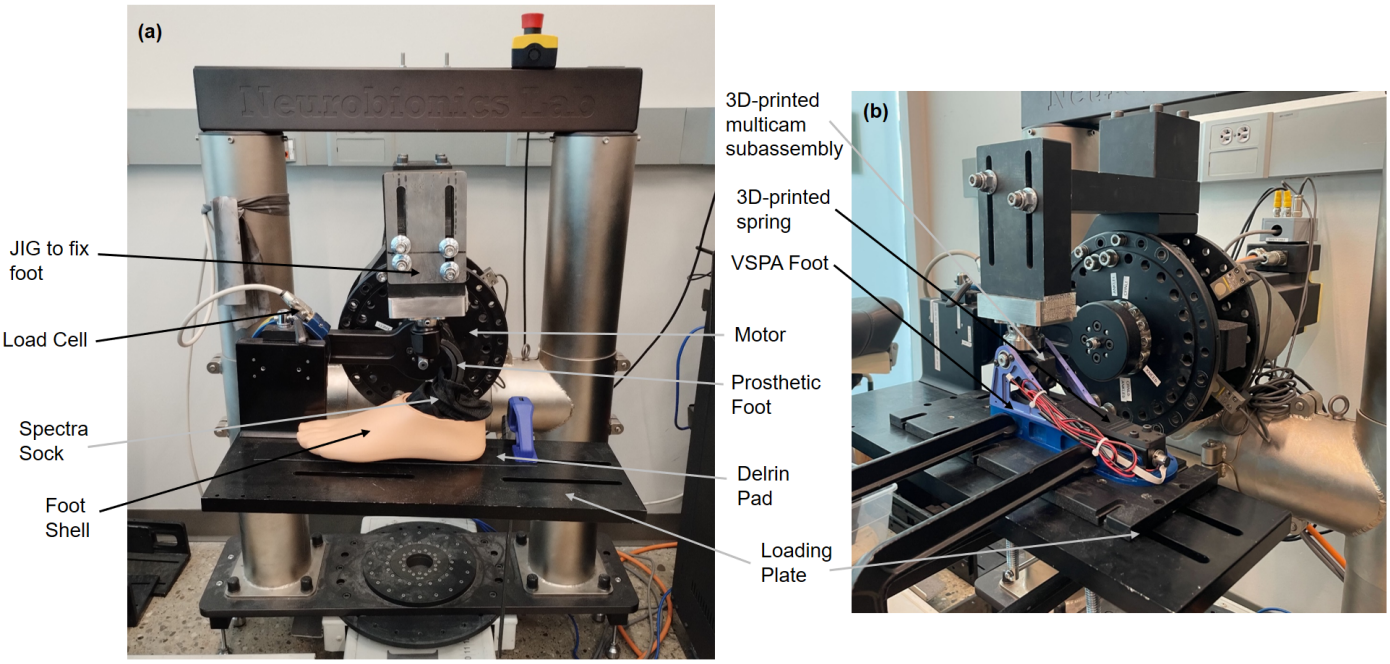

Figure 9: Setup for mechanical characterisation of the prostheses and the VSPA foot: (a) Experimental characterisation of the mechanical properties for the AllPro prosthetic foot using the custom-built dynamometer. The prosthesis is fitted with a spectra sock and its corresponding footshell. The jig keeps the superior part of the prosthesis stationary. The loading platform rotates the feet to the desired range of motion simulating dorsiflexion and plantarflexion. The torque is measured by the six-axis load cell. (b) Experimental characterisation of the VSPA foot fitted with the 3D-printed multicam subassembly on the dynamometer. A ±15°range of motion of the ankle joint was implemented. The other boundary conditions for the VSPA foot characterisation were kept similar to those of the passive-elastic prosthetic feet. The reaction torque was measured using the load cell.

terworth filter with a 12 Hz cutoff frequency was then applied to eliminate high-frequency noise. To convert the filtered, discrete torque-angle data into a continuous function, a power regression model was employed, shown below, where T represents the measured torque in Nm, θ the angle of rotation in radians, a the intercept and b the power coefficient.

$$T = a\theta^b \text{.....(1)}$$

The intercept a and power coefficient b were determined by fitting the regression model to the torque-angle data. To validate the model, adjusted R^2 values were calculated, as these account for additional dofs in the model. Using the estimated continuous functions, the ankle range of motion (ROM) for all prosthetic feet was extended to ±40°in dorsiflexion and plantarflexion. This adjustment facilitates consistent testing of each foot while aligning with the biological ROM of the human ankle. The loading phase of the torque-angle function was used as input to a mathematical algorithm, initially developed by Shepherd and Rouse (2017), to generate the corresponding cam profiles [22]. During post-processing, each cam profile was divided into dorsiflexion, plantarflexion, and central shared curves. The central curve was obtained by averaging the curves within ±2.5 mm of the equilibrium point across all cam profiles. Dorsiflexion and plantarflexion curves were then interpolated to ensure a smooth intersection with the central curve.

3.2. FEA of the Multicam Mechanism

Finite Element Analysis (FEA) was employed in ANSYS Workbench (Ansys®, PA, USA) to predict potential mechanical failure in the design. During meshing, the multicam subassembly was discretized into 4-noded tetrahedral elements with 10 degrees of freedom. A mesh sensitivity study was conducted to identify the optimal element size with respect to computational efficiency. To determine the reaction force and Von Mises stress at the top face where the pyramid adapter connects, FE models with element sizes of 1 mm, 1.5 mm, and 2 mm were constructed. The relative difference in reaction force was 1.02% between mesh sizes of 2 mm and 1.5 mm and further reduced to 0.68% when reduced to 1 mm. Although the model with a 1 mm mesh size provided slightly improved accuracy, it incurred a 66.67% increase in computational time relative to the 1.5 mm model. Thus, a 1.5 mm element size was selected for the final simulations.

Maximum normal reaction forces on the cam profile are exerted by the cam follower at the extreme points in the ROM during both dorsiflexion and plantarflexion cycles. By dividing the ankle torque at these extreme positions by the corresponding moment arms, the normal reaction forces exerted on the cam profile during dorsiflexion and plantarflexion were determined. To simulate the custom-built dynamometer, all degrees of freedom in the top part of the subassembly, where the pyramid adapter is attached, were constrained. The maximum dorsiflexion and plantarflexion loads were applied at the ends of the cam profile. While theoretically, the contact between the cam and follower is line contact, a small area ($1.1x10^{-3}$) was assumed to prevent stress concentration artefacts. The subassembly's bottom frame was restricted to rotation about the ankle axis (global

z-axis), and frictional contact was simulated, with coefficients of dynamic friction set to 0.4 between tool steel parts and 0.8 between aluminium and tool steel. Von Mises stress was used as the primary indicator of potential failure within the subassembly.

The torque-angle characteristics exhibited by the cam profiles in the design were also evaluated via FEA and subsequently compared to experimental data. To reduce the computational cost, the VSPA foot model was simplified (Figure 13), removing the frame while retaining the leaf spring, cam follower, and slider pin to regulate the simple support position on the spring. The deflection of the spring was assessed by rotating the multicam subassembly about the ankle axis to simulate dorsiflexion and plantarflexion cycles. Similar results to the previous FEA analysis were obtained in a mesh sensitivity study, confirming the selection of a 1.5 mm element size with 4-noded tetrahedral elements.

Titanium was assigned to the leaf spring, while A8 tool steel was used for both the cam follower and slider pin. Material assignments for other subassembly components were consistent with previous simulations. Boundary conditions fixed one end of the leaf spring to simulate cantilever loading. The slider pin was positioned and fixed at the primary slider position, following Shepherd and Rouse's model [22]. The multicam subassembly frame was rotated about the ankle axis (global z-axis) from +15°to -15°, simulating dorsiflexion and plantarflexion relative to the equilibrium position (ankle angle = 0°). Angular displacement of the frame was applied iteratively at 0.1515°per second.

To determine the ankle torque, the reaction force (F_c) was obtained at the leaf spring's fixed end (Figure 10). Using rotational equilibrium, the moment M_S deflecting the spring about the simple support was calculated using Equation 2 where l_c and l_a are the moment arms to the loading (A) and the fixed (C) ends, and F_c is the normal force exerted by the cam on the follower. Assuming no energy loss in transmission or spring, the concept of virtual work was applied to equate energy stored at the ankle and in the leaf spring as expressed in Equation 3, where γ is the angular deflection of the spring,θ the ankle angle, δ the series compliance of the subassembly and M_A the ankle torque. The deflection angle γ was calculated from the spring's vertical displacement and effective length per Equation 4 where y is the vertical displacement of the spring. Deformation of the subassembly δ was calculated from the averaged displacement of 20 nodes on the multicam frame using the probe tool.

$$M_S = F_c l_c = F_a l_a \text{.....(2)}$$

$$\int_0^{\gamma} M_S \, d\gamma = \int_0^{\theta} M_A \, d\theta - \int_0^{\delta} M_A \, d\delta \text{.....(3)}$$

$$\gamma = \frac{y}{l_a} \text{.....(4)}$$

FEA-predicted torque was plotted against the input ankle angle to obtain the torque-angle relationship (Figure 13(b)).

3.3. Experimental Evaluation of the VSPA Multicam Foot

The Multicam subassembly and leaf spring components were 3D printed using Onyx® (a composite material with a nylon matrix reinforced by microcarbon fibers) by Markforged, allowing for initial design evaluation and torque-angle curve estimation (Figure 11). To enhance print quality, several modifications were applied. Overhangs exceeding 45°were minimized to prevent excessive support structures, which could impair surface finish and necessitate extensive post-processing. Complex shapes and intricate details were simplified to improve compatibility with the 3D printer and reduce the likelihood of errors. Component orientations were adjusted to minimize support material and maximize structural integrity along the loading axis in the sagittal plane. Tolerances were refined to match the 3D printer's capabilities and ensure proper component fit within the assembly, with 0.2 mm used for normal fits and 0.1 mm for tighter fits based on the printer's 0.1 mm layer height preset. To facilitate assembly, the cam barrel housing was split into two parts, subsequently joined with super glue. Locating features on the halves were omitted to prevent overhangs, with bolts added to support vertical loads. Additionally, the leaf spring and associated interacting components were 3D printed, as initial iterations using a titanium spring led to plastic deformation of the printed subassembly.

The functionality of the VSPA Multicam foot was evaluated using a dynamometer to estimate the torque-angle curves. The prosthetic foot was subjected to ±15°in dorsiflexion and plantarflexion cycles. Initially, a dry run (without spring engagement) was conducted to isolate torque contributions from the dynamometer and VSPA foot components. Subsequently, torque-angle data were recorded with the Variflex cam profile engaged. Dry-run torque was subtracted from the engaged-torque values to determine the prosthetic's true dynamic response. Torque-angle data were collected at various spring stiffnesses, modulated by altering the spring's slider support position. To refine data from the emulated Variflex foot, the torque-angle values were filtered using three tenth-order notch filters spaced at 30 Hz increments, with an 8 Hz bandwidth, and a second-order Butterworth filter at a 12 Hz cutoff to remove high-frequency noise.

4. Results

4.1. Characterisation of the Commercial Prosthetic Feet

A non-linear relationship between the measured torque and the input ankle rotation angle was observed across all tested commercial prosthetic feet, with each foot demonstrating a unique range of effective torsional stiffness. Overall, the passive-elastic prostheses exhibited a stiffening behaviour, as evidenced by the concave-up shape of the torque-angle curves. Significant hysteresis losses were detected in the plantarflexion cycle for all feet. In the case of the Fillauer All-Pro foot (Stiffness Category: D6), a pronounced increase in reaction torque was observed once the ankle angle exceeded 12°, as depicted in Figure 12. During the unloading phase of the plantarflexion cycle, higher reaction torque was recorded within the initial 5°range of motion, after which the torque readings approached zero and maintained this level through the remainder of the cycle. This distinctive response was noted across multiple trials and indicates

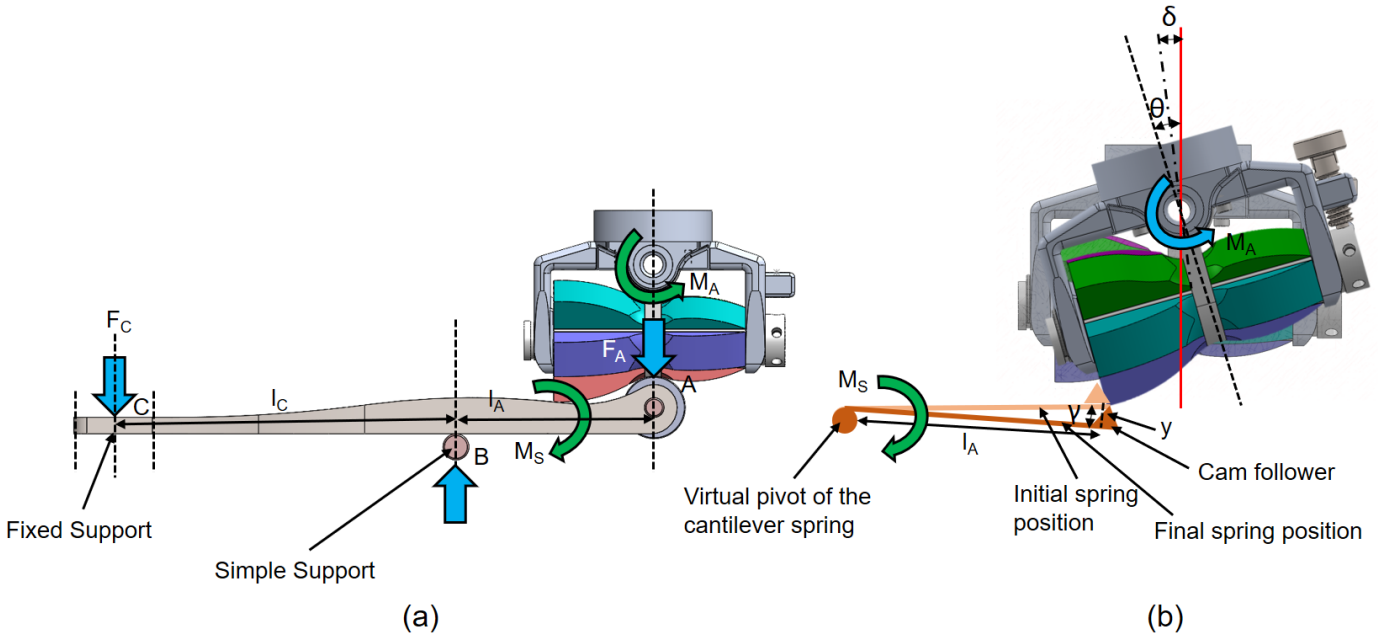

Figure 10: Boundary conditions and the input/output parameters for deriving the ankle torque-angle curves for a cam profile: (a) FEA boundary conditions for predicting the torque-angle characteristics of the cam profiles. The end of the leaf spring is fixed to simulate a cantilever loading. The slider (simple support) is fixed at the primary slider position. Ankle range of motion (θ) for the dorsiflexion and plantarflexion motions is applied about the ankle axis as angular displacements. (b) The leaf spring can be approximated as a rotary spring rotating about the virtual pivot point (the slider position). As the cam subassembly rotates the spring deflects from the initial to the final position by an angle γ and vertically by a distance y. δ is the deformation angle of the subassembly frame.

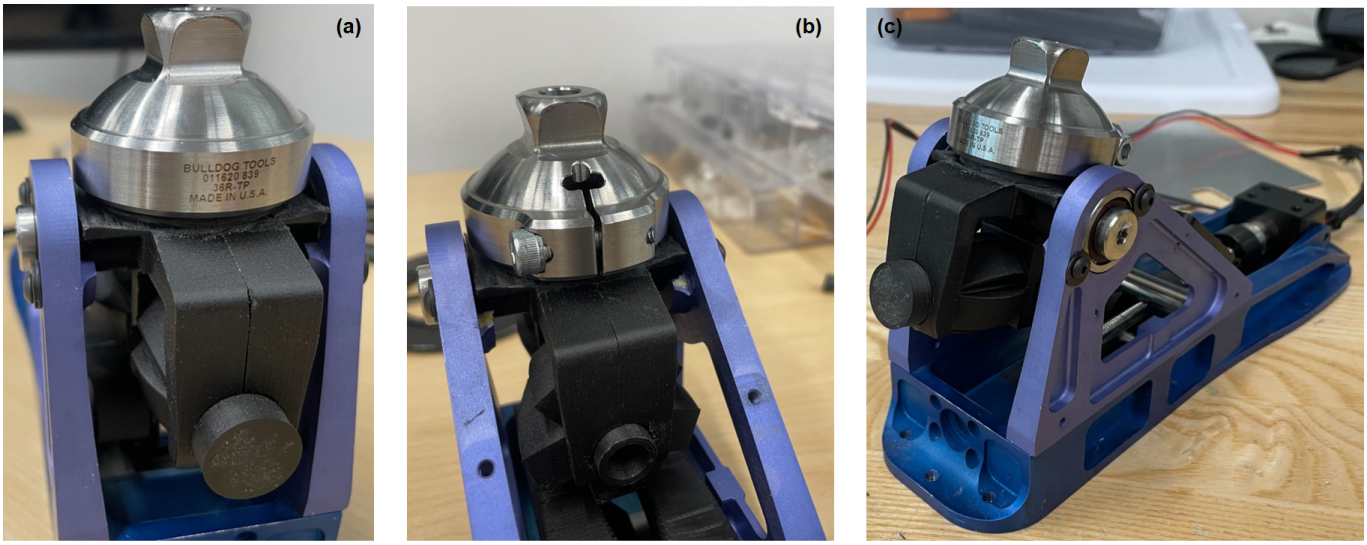

Figure 11: The 3D-printed multicam subassembly inserted in the VSPA foot: (a) Posterior view, (b) Anterior view and (c) Isometric view.

specific mechanical characteristics unique to the prosthetic foot design.

4.2. FEA of the Multicam Mechanism

FEA was employed to evaluate the designed multicam subassembly for potential yielding or fracture using Von Mises stress as a failure criterion. Under dorsiflexion loading conditions, the maximum stress value recorded (2663.3 MPa) was localized in the region of applied load on the cam profile (Figure 13(a)). This stress level remained substantially below the yield strength of A8 Tool Steel, thereby indicating that the subassembly is structurally robust and capable of bearing the anticipated loads. Similarly, under plantarflexion loading, the maximum stress observed (1107.2 MPa) was localized at the load application site and fell well below the material's yield threshold.

To further validate the design's capability in replicating the experimentally determined torque-angle characteristics of the prosthetic feet, ankle torques produced by the designed cam

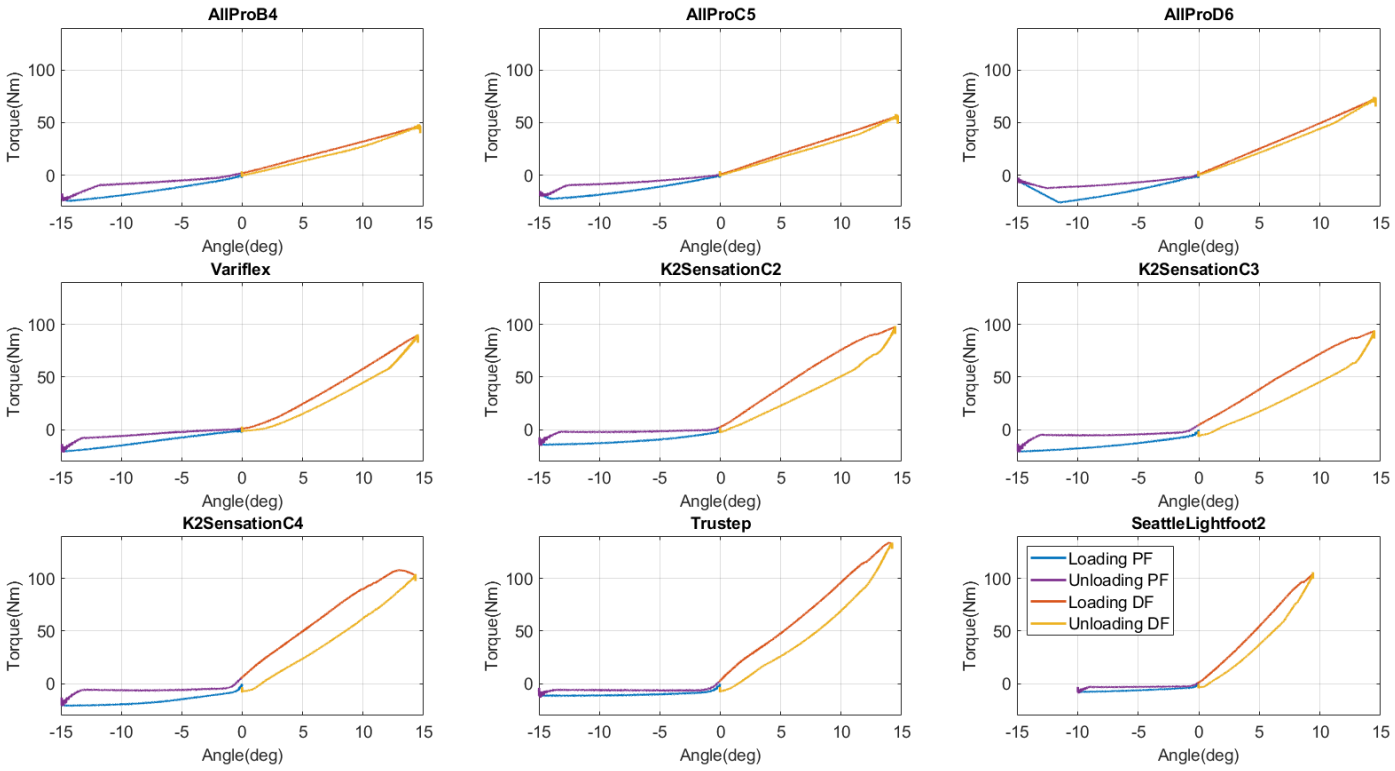

Figure 12: Ankle torque-angle characteristics from mechanical testing of the passive-elastic feet during the dorsiflexion (DF) and plantarflexion (PF) loading and unloading cycles.

profiles in both dorsiflexion and plantarflexion were evaluated through FEA (Figure 13(b)). Percentage error between the experimentally derived torque values and those predicted by FEA was calculated for both loading cycles. The dorsiflexion and plantarflexion cycles yielded percentage errors of 2.87% and 9.28%, respectively, demonstrating a high degree of accuracy in the emulated torque response generated by the cam profiles.

4.3. Experimental Evaluation of the VSPA Multicam Foot

The torque-angle curves generated from mechanical testing of the emulated Variflex foot were compared with experimentally derived data from the actual Variflex prosthesis. Due to the notably low stiffness of the cantilever spring, only the emulated torque-angle curve corresponding to the highest stiffness setting—achieved by positioning the slider closest to the cam profile's equilibrium point—was selected for comparison with the actual prosthetic data. Similar concave-up profiles in the torque-angle curves indicated consistent stiffening behavior in the emulated foot, mirroring the response observed in the experimental data. The reduction in output torque, however, was substantial and can be attributed to differences in material properties between the 3D-printed spring, the multicam subassembly, and the intended design materials. An isolated oscillation was detected in the torque measurements over an approximate 2.5°range of motion in the dorsiflexion loading phase, which could potentially be attributed to minor machine calibration discrepancies (Figure 14(a)). Additionally, when comparing torque-angle curves resulting from adjustments in spring stiffness (achieved by modifying the simple support slider position), an increase in the primary torque-angle slope was observed with higher stiffness settings, while the opposite trend was noted for lower stiffness settings (Figure 14(b)).

5. Discussion

In this study, a novel ankle prosthesis emulator based on the VSPA foot design was presented and validated. The emulator is capable of rapid, manual back-to-back testing of five distinct passive-elastic prosthetic feet by enabling manual rotation of the cam barrel at a 0°ankle angle. To validate the emulator's effectiveness, the multicam subassembly was 3D-printed, and the resultant ankle torque-angle relationships were characterized and subsequently compared to experimental data obtained from corresponding actual prostheses. The required and achieved design specifications are listed in Table 3.

To emulate the mechanical behaviours of commonly prescribed passive-elastic prosthetic feet, mechanical testing was utilized to determine each foot's torque-angle characteristics. Alternatively, these characteristics could be derived from kinematic and kinetic data collected from users with prosthetic feet during gait analysis [33]. However, gait deviations and compensatory strategies frequently observed in individuals with transtibial amputation introduce variability that may affect the accurate measurement of foot stiffness, influenced by factors specific to each user [34, 35]. Consequently, mechanical testing was chosen to provide a controlled and efficient approach to evaluating prosthetic foot properties, independent of user variability [30, 36].

Table 3: Overview of the Fulfilment of the Design Requirements

Criteria	Parameter	Requirement	Fulfilment
Functional	Emulating the passive-elastic prostheses	Within <5% estimation of torque-angle curves of the prostheses with the VSPA multicam foot.	Not satisfied
	Number of cam profiles	Number of cams > 3	Satisfied Number of cams = 5
	Quasi-passive	Maintain stiffness variability feature of the VSPA foot	Satisfied
	Mass	Overall weight of the multicam subassembly and the VSPA foot should not exceed 1.5kg	Not satisfied The final overall weight of the multicam subassembly and the VSPA foot based on the CAD model is 1.63kg; not satisfied
	Range of Motion	Range of Motion of the emulator: >20° in plantarflexion and >15° in dorsiflexion	Satisfied Range of Motion of the emulator: 40° in plantarflexion and 40° in dorsiflexion
	Dimentional constraint	Distance from the ankle axis to the equilibrium point = 43.5mm	Satisfied
	Transition time	Transition time between two sequential cams should be <2s	Satisfied Transition time between two sequential cams = 1.3s
General	Customisability	The mechanism should accommodate emulated prosthetic feet from different stiffness categories, sizes and functional support	Satisfied In the mechanism, cams are swappable so all patient preferences and requirements can be satisfied
	Modularity	The mechanism should be easily (dis)assembled	Satisfied Removing the barrel pin results in instant disassembly of the components and viceversa
	Off-the-shelf components	Off-the-shelf components should be used to lower the cost	Satisfied Spring plunger used to secure the barrel pin is Off-the-shelf

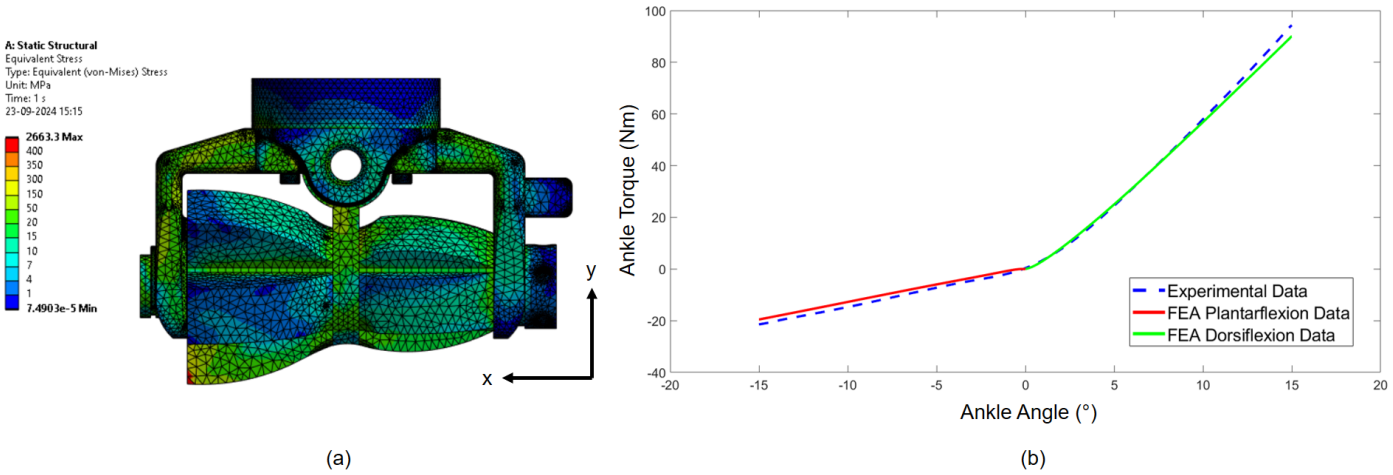

Figure 13: Results for the FEA of the multicam mechanism: (a) Von Mises stress distribution observed in the subassembly for the maximum load during the dorsiflexion cycle. The maximum Von Mises stress is located at the loading area on the dorsiflexion cam. The magnitude is significantly less than the yield stress of the constructing material; A8 tool steel, indicating no plastic deformation. (b) Comparison between the FEA predicted and the experimentally obtained torque-angle curves for the Variflex foot. The closeness of the data shows that the FEA predicted the experimental data accurately

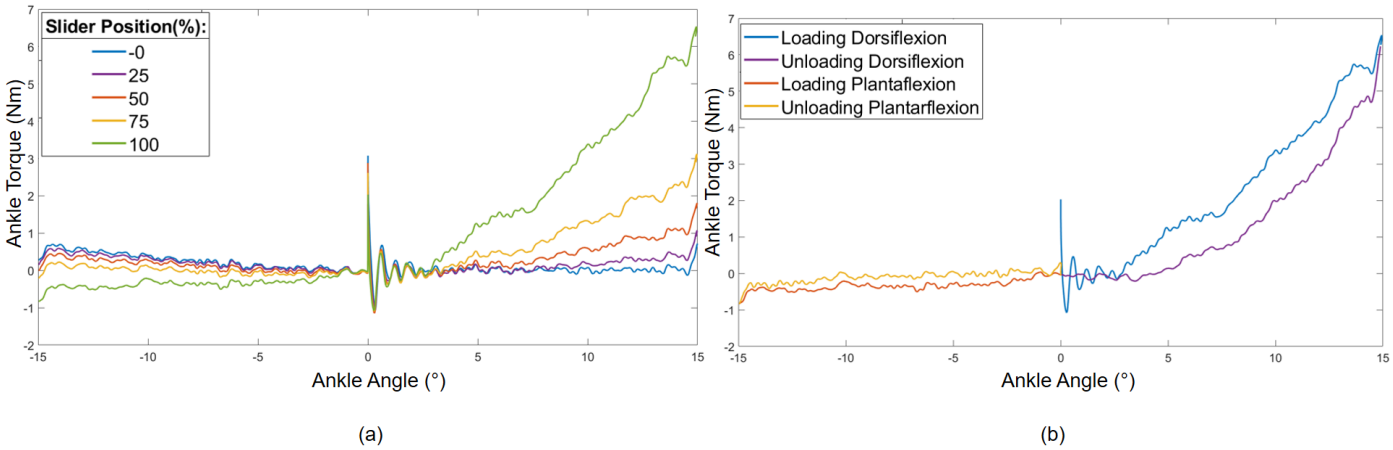

Figure 14: Results for the experimental characterisation of the VSPA foot fitted with the 3D-printed multicam subassembly: (a) Emulated torque-angle curves of Variflex foot across different spring stiffnesses obtained by sliding the simple support position. The slider position (%) indicates the spring stiffness; 0% indicates the least stiff spring stiffness and 100% indicates the highest. (b) Ankle torque-angle curves for the emulated Variflex prosthetic foot during dorsiflexion and plantarflexion loading and unloading of the 3D-printed cam profile.

The non-linear relationship observed between ankle torque and angle was well described by a power function. Across all prosthetic feet and stiffness categories, the power function exhibited high statistical reliability, with adjusted R^2 values averaging 0.95 ± 0.1 (mean ± standard deviation). The stiffening behaviour noted during dorsiflexion and plantarflexion cycles was likely due to the arched design of the prosthetic feet, which limited the loading platform's contact area to specific regions of the forefoot and hindfoot [30]. Consistent positioning of the ankle axis across all prosthetic feet and the VSPA emulator was maintained by not altering the rotation axis. The resulting torque-angle characteristics—characterized by stiffening behaviour during dorsiflexion and plantarflexion—are consistent with findings from prior experimental studies on prosthetic foot characterization [30, 31]. Halsne et al. (2022) utilized a 6DOF R2000 Rotopod parallel robot (Mikrolar, Inc.; Hampton, NH) to simulate uniaxial loading of a prosthetic foot attached to a top-mounted loading plate that followed a human ankle trajectory [31]. Similarly, Tacca et al. (2024) employed a materials testing machine (Instron Series 5859, Norwood, MA) to characterize low-profile Variflex prostheses under uniaxial torsional load, applied using a custom fixture in the compression testing setup [30]. Comparable torque-angle responses across these studies validate the mechanical characterization approach employed in this investigation.

Material selection for the multi-cam subassembly was prioritized to minimize weight while ensuring durability. 7075 Aluminum was selected for the cam barrel housing due to its favorable strength-to-weight ratio and the negligible localized stress revealed in FEA. For components experiencing higher wear, such as the cam follower and barrel pin, A8 Tool Steel was chosen for its durability and resistance to wear, essential for

the cam follower's sustained contact with the cam profile during stance phases. The barrel pin, which lacks vertical support, was fabricated from Tool Steel to resist potential buckling. Future research may involve optimization routines to further enhance the subassembly's design, potentially reducing weight without compromising durability.

The FEA analysis subjected the multicam subassembly to maximum loads encountered during dorsiflexion and plantarflexion. These loads, derived from ankle torque measurements obtained from the prosthetic feet tested with the custom dynamometer, confirmed the absence of yielding or fracture in any subassembly component. Furthermore, the FEA-predicted torque-angle behaviour for each cam profile was compared with experimentally measured torque across dorsiflexion and plantarflexion ranges. Low percentage errors between FEA predictions and experimental data demonstrate that the cam profiles effectively replicate the mechanical characteristics of the emulated prosthetic feet.

Onyx®, a composite material, was chosen for 3D printing due to its ability to produce parts with superior surface finish and relative dimensional accuracy. This material also exhibited stiffness approximately 1.4 times greater than traditional ABS [37]. For the experimental setup, the titanium leaf spring was replaced with a more compliant 3D-printed spring to reduce the normal forces exerted on the multicam subassembly. The 3D-printed tolerances facilitated smooth cam barrel rotation between the five cam profiles, demonstrating the efficacy of the proposed design.

When emulating the Variflex foot's torque-angle characteristics, the 3D-printed cam profile did not fully replicate the measured torque values observed with the actual prosthesis. This discrepancy is likely due to the differences in mechanical properties between the materials in the 3D-printed subassembly and the proposed materials. The 3D-printed spring exhibited considerable compliance even in its stiffest configuration, resulting in increased deflection. Modifications to the design, necessary for 3D printing, may have also influenced the observed performance. The isolated oscillation observed in the dorsiflexion loading cycle across all stiffness settings, including the dry run, suggests a potential calibration error within the testing machine. Despite these variations, the fundamental mechanism of the rotating multicam design was successfully demonstrated, and the comparable shape of the emulated torque-angle data suggests that emulating the mechanical behaviour of passive-elastic prosthetic feet is achievable. Optimal performance is expected once components are manufactured with the proposed materials, which should also address the frictional forces observed as the cam follower slid rather than rolled during engagement with the cam profile. This issue is anticipated to be resolved with improved material selection in future builds.

6. Limitations and Future Scope

During mechanical characterization, contact with the prosthetic foot occurred only at localized regions in the forefoot and hindfoot areas during dorsiflexion and plantarflexion, respectively. This setup did not replicate the centre of pressure (COP) trajectory typically seen in the walking gait of a unilateral transtibial amputee [38]. Future research should explore setups that more accurately mimic COP progression across the gait cycle with prosthetic feet. Achieving this may require preloading the prosthesis with half of the manufacturer-recommended body weight and adjusting the position of the ankle axis of rotation [39, 40].

In addition, the 3D-printed multicam subassembly used in this study did not fully replicate the ankle torque-angle characteristics of commercial prosthetic feet, largely due to differences between the proposed materials and the 3D-printed Onyx® filament. Consequently, further evaluations should be conducted using the subassembly manufactured from the materials specified in the proposed design.

The novel multicam mechanism presented here holds potential applications beyond testing; it could also serve in adaptive quasi-passive ankle prostheses. By designing cam profiles to replicate terrain-dependent torque-angle characteristics (e.g., flat terrain walking, stair ascent/descent, standing, and running), and using a user intent recognition algorithm, the mechanism could dynamically adjust cam profiles based on the required ambulatory task. This adaptive capability would allow the prosthesis to more accurately mimic able-bodied ankle biomechanics.

7. Conclusion

A novel ankle prosthetic emulator was proposed and tested for the rapid assessment of multiple clinically prescribed passive-elastic prosthetic feet. Five commercial prosthetic feet were characterized to establish their ankle torque-angle relationships, and power functions were developed to model these relationships with high statistical accuracy.

FEA simulations demonstrated that none of the design components exhibited yielding, thereby validating the load-bearing capacity of the multicam mechanism. The efficacy of the proposed design in emulating prosthetic foot mechanics was confirmed by the low percentage error between FEA-predicted and experimentally derived torque-angle data. The 3D-printed multicam subassembly produced comparable torque-angle curve shapes in mechanical testing, supporting the design's capability to emulate passive-elastic prosthetic foot behaviour. Differences in torque magnitudes are attributed to the material discrepancies between the 3D-printed and intended materials, an issue expected to be resolved in future manufacturing efforts using the specified materials and processes.

8. Acknowledgment

The author would like to express his deepest gratitude to his daily supervisor, Elliott J. Rouse, for serving as a project mentor and providing invaluable guidance throughout this project. Special thanks are also extended to the thesis supervisor, Gerwin Smit, for his insights into the mechanical design aspects, constructive feedback on the project's progress, and for facilitating seamless communication between the University of Michigan

and Delft University of Technology. His feedback on the writing and interim presentations was instrumental in shaping this work. The author is also grateful to the members of the Neurobionics Lab, particularly Nikko Van Crey and David Lam, for their valuable input on the mechanical and conceptual design aspects of the project and their assistance in acquiring testing data from the Joint Impedance Machine (JIM), the rotary dynamometer used for foot characterization. Finally, heartfelt thanks go to the author's friends and family for their unwavering support and encouragement throughout this journey.

References

[1] Kathryn Ziegler-Graham et al. "Estimating the Prevalence of Limb Loss in the United States: 2005 to 2050". In: *Archives of Physical Medicine and Rehabilitation* 89.3 (Mar. 2008), pp. 422–429. ISSN: 00039993. DOI: 10.1016/j.apmr.2007.11.005.

[2] J.P. Pell et al. "Quality of life following lower limb amputation for peripheral arterial disease". In: *European Journal of Vascular Surgery* 7.4 (July 1993), pp. 448–451. ISSN: 0950821X. DOI: 10.1016/S0950-821X(05)80265-8.

[3] Andra Cătălina Roșca et al. "Psychological Consequences in Patients With Amputation of a Limb. An Interpretative-Phenomenological Analysis". In: *Frontiers in Psychology* 12 (May 26, 2021), p. 537493. ISSN: 1664-1078. DOI: 10.3389/fpsyg.2021.537493.

[4] K Sansam et al. "Predicting walking ability following lower limb amputation: A systematic review of the literature". In: *Journal of Rehabilitation Medicine* 41.8 (2009), pp. 593–603. ISSN: 1650-1977. DOI: 10.2340/16501977-0393.

[5] Richa Gupta et al. "Ankle and Foot Arthroplasty and Prosthesis: A Review on the Current and Upcoming State of Designs and Manufacturing". In: *Micromachines* 14.11 (Nov. 10, 2023), p. 2081. ISSN: 2072-666X. DOI: 10.3390/mi14112081.

[6] Elke Lathouwers et al. "Evaluation of an articulated passive ankle–foot prosthesis". In: *BioMedical Engineering OnLine* 21.1 (Dec. 2022), p. 28. ISSN: 1475-925X. DOI: 10.1186/s12938-022-00997-6.

[7] Adan Domínguez-Ruiz et al. "Low limb prostheses and complex human prosthetic interaction: A systematic literature review". In: *Frontiers in Robotics and AI* 10 (Feb. 13, 2023), p. 1032748. ISSN: 2296-9144. DOI: 10.3389/frobt.2023.1032748.

[8] Cleveland Barnett et al. "Kinematic Gait Adaptations in Unilateral Transtibial Amputees During Rehabilitation". In: *Prosthetics & Orthotics International* 33.2 (June 2009), pp. 135–147. ISSN: 0309-3646. DOI: 10.1080/03093640902751762.

[9] Patrick G. Monaghan et al. "Characterization of initial ankle-foot prosthesis prescription patterns in U.S. Service members following unilateral transtibial amputation". In: *Frontiers in Rehabilitation Sciences* 4 (Aug. 25, 2023), p. 1235693. ISSN: 2673-6861. DOI: 10.3389/fresc.2023.1235693.

[10] Harmen Van Der Linde et al. "A systematic literature review of the effect of different prosthetic components on human functioning with a lower-limb prosthesis". In: *The Journal of Rehabilitation Research and Development* 41.4 (2004), p. 555. ISSN: 0748-7711. DOI: 10.1682/JRRD.2003.06.0102.

[11] Brian J. Hafner et al. "Effects of prosthetic feet on metabolic energy expenditure in people with transtibial amputation: A systematic review and meta-analysis". In: *PM&R* 14.9 (Sept. 2022), pp. 1099–1115. ISSN: 1934-1482, 1934-1563. DOI: 10.1002/pmrj.12693.

[12] Joseph M. Czerniecki. "Research and Clinical Selection of Foot-Ankle Systems:" in: *JPO Journal of Prosthetics and Orthotics* 17 (Supplement Oct. 2005), S35–S37. ISSN: 1040-8800. DOI: 10.1097/00008526-200510001-00012.

[13] Phillip M. Stevens, John Rheinstein, and Shane R. Wurdeman. "Prosthetic Foot Selection for Individuals with Lower-Limb Amputation: A Clinical Practice Guideline". In: *JPO Journal of Prosthetics and Orthotics* 30.4 (Oct. 2018), pp. 175–180. ISSN: 1040-8800. DOI: 10.1097/JPO.0000000000000181.

[14] H. Van Der Linde et al. "Prosthetic prescription in the Netherlands: An observational study". In: *Prosthetics & Orthotics International* 27.3 (Dec. 2003), pp. 170–178. ISSN: 0309-3646. DOI: 10.1080/03093640308726679.

[15] Chelsey B. Anderson et al. "Understanding decision-making in prosthetic rehabilitation by prosthetists and people with lower limb amputation: a qualitative study". In: *Disability and Rehabilitation* 45.4 (Feb. 13, 2023), pp. 723–732. ISSN: 0963-8288, 1464-5165. DOI: 10.1080/09638288.2022.2037745.

[16] Cheriel J Hofstad et al. "Prescription of prosthetic ankle-foot mechanisms after lower limb amputation". In: *Cochrane Database of Systematic Reviews* 2010.1 (Jan. 26, 2004). Ed. by Cochrane Bone, Joint and Muscle Trauma Group. ISSN: 14651858. DOI: 10.1002/14651858.CD003978.pub2.

[17] Silvia U. Raschke et al. "Biomechanical characteristics, patient preference and activity level with different prosthetic feet: A randomized double blind trial with laboratory and community testing". In: *Journal of Biomechanics* 48.1 (Jan. 2015), pp. 146–152. ISSN: 00219290. DOI: 10.1016/j.jbiomech.2014.10.002.

[18] Joshua M. Caputo and Steven H. Collins. "A Universal Ankle–Foot Prosthesis Emulator for Human Locomotion Experiments". In: *Journal of Biomechanical Engineering* 136.3 (Mar. 1, 2014), p. 035002. ISSN: 0148-0731, 1528-8951. DOI: 10.1115/1.4026225.

[19] Anthony Anderson et al. *Design, Control, and Evaluation of a Robotic Ankle-Foot Prosthesis Emulator*. Sept. 21, 2023. DOI: 10.36227/techrxiv.20352861.

[20] Steven H. Collins et al. "An ankle-foot prosthesis emulator with control of plantarflexion and inversion-eversion torque". In: *2015 IEEE International Conference on Robotics and Automation (ICRA)*. 2015 IEEE International Conference on Robotics and Automation (ICRA). Seattle, WA: IEEE, May 2015, pp. 1210–1216. ISBN: 978-1-4799-6923-4. DOI: 10.1109/ICRA.2015.7139345.

[21] Joshua Caputo, Peter Adamczyk, and Steve Collins. *Informing ankle-foot prosthesis prescription through haptic emulation of candidate devices*. 2015. DOI: 10.13140/RG.2.1.3738.5768.

[22] Max K. Shepherd and Elliott J. Rouse. "The VSPA Foot: A Quasi-Passive Ankle-Foot Prosthesis With Continuously Variable Stiffness". In: *IEEE Transactions on Neural Systems and Rehabilitation Engineering* 25.12 (Dec. 2017), pp. 2375–2386. ISSN: 1534-4320, 1558-0210. DOI: 10.1109/TNSRE.2017.2750113.

[23] Niels Jonkergouw et al. "The Effect of Alignment Changes on Unilateral Transtibial Amputee's Gait: A Systematic Review". In: *PLOS ONE* 11.12 (Dec. 6, 2016). Ed. by Steven Allen Gard, e0167466. ISSN: 1932-6203. DOI: 10.1371/journal.pone.0167466.

[24] Nahid Tafti et al. "A systematic review of variables used to assess clinically acceptable alignment of unilateral transtibial amputees in the literature". In: *Proceedings of the Institution of Mechanical Engineers, Part H: Journal of Engineering in Medicine* 232.8 (Aug. 2018), pp. 826–840. ISSN: 0954-4119, 2041-3033. DOI: 10.1177/0954411918789450.

[25] Tyler R. Clites et al. "Understanding patient preference in prosthetic ankle stiffness". In: *Journal of NeuroEngineering and Rehabilitation* 18.1 (Aug. 25, 2021), p. 128. ISSN: 1743-0003. DOI: 10.1186/s12984-021-00916-1.

[26] Erica A. Hedrick et al. "The effects of ankle stiffness on mechanics and energetics of walking with added loads: a prosthetic emulator study". In: *Journal of NeuroEngineering and Rehabilitation* 16.1 (Dec. 2019), p. 148. ISSN: 1743-0003. DOI: 10.1186/s12984-019-0621-x.

[27] Gabriele Bovi et al. "A multiple-task gait analysis approach: Kinematic, kinetic and EMG reference data for healthy young and adult subjects". In: *Gait & Posture* 33.1 (Jan. 2011), pp. 6–13. ISSN: 09666362. DOI: 10.1016/j.gaitpost.2010.08.009.

[28] Emily Rogers-Bradley et al. “Design and Evaluation of a Quasi-Passive Variable Stiffness Prosthesis for Walking Speed Adaptation in People With Transtibial Amputation”. In: *IEEE/ASME Transactions on Mechatronics* 29.1 (Feb. 2024), pp. 335–346. ISSN: 1083-4435, 1941-014X. DOI: 10.1109/TMECH.2023.3276710.

[29] Hashim A. Quraishi et al. “A passive mechanism for decoupling energy storage and return in ankle–foot prostheses: A case study in recycling collision energy”. In: *Wearable Technologies* 2 (2021), e9. ISSN: 2631-7176. DOI: 10.1017/wtc.2021.7.

[30] Joshua R. Tacca, Zane A. Colvin, and Alena M. Grabowski. “Low-profile prosthetic foot stiffness category and size, and shoes affect axial and torsional stiffness and hysteresis”. In: *Frontiers in Rehabilitation Sciences* 5 (Feb. 28, 2024), p. 1290092. ISSN: 2673-6861. DOI: 10.3389/fresc.2024.1290092.

[31] Elizabeth G. Halsne et al. “Emulating the Effective Ankle Stiffness of Commercial Prosthetic Feet Using a Robotic Prosthetic Foot Emulator”. In: *Journal of Biomechanical Engineering* 144.11 (Nov. 1, 2022), p. 111009. ISSN: 0148-0731, 1528-8951. DOI: 10.1115/1.4054834.

[32] Matthew J. Major et al. “Effects of women’s footwear on the mechanical function of heel-height accommodating prosthetic feet”. In: *PLOS ONE* 17.1 (Jan. 24, 2022). Ed. by Arezoo Eshraghi, e0262910. ISSN: 1932-6203. DOI: 10.1371/journal.pone.0262910.

[33] Selin Aydin Fandakli, Halil Ibrahim Okumus, and Mehmet Ozturk. “A Study of Human Walking Biomechanics for Ankle-Foot Prosthesis Design”. In: *2018 6th International Conference on Control Engineering & Information Technology (CEIT)*. 2018 6th International Conference on Control Engineering & Information Technology (CEIT). Istanbul, Turkey: IEEE, Oct. 2018, pp. 1–5. ISBN: 978-1-5386-7641-7. DOI: 10.1109/CEIT.2018.8751801.

[34] Arezoo Eshraghi et al. “Gait Biomechanics of Individuals with Transtibial Amputation: Effect of Suspension System”. In: *PLoS ONE* 9.5 (May 27, 2014). Ed. by Alfonso Fasano, e96988. ISSN: 1932-6203. DOI: 10.1371/journal.pone.0096988.

[35] Deanna H. Gates et al. “Gait characteristics of individuals with transtibial amputations walking on a destabilizing rock surface”. In: *Gait & Posture* 36.1 (May 2012), pp. 33–39. ISSN: 09666362. DOI: 10.1016/j.gaitpost.2011.12.019.

[36] M. Sam, A.H. Hansen, and D.S. Childress. “Mechanical characterization of prosthetic feet using a Prosthetic Foot Loading Apparatus”. In: *Proceedings of the 22nd Annual International Conference of the IEEE Engineering in Medicine and Biology Society (Cat. No.00CH37143)*. 22nd Annual International Conference of the IEEE Engineering in Medicine and Biology Society. Vol. 3. Chicago, IL, USA: IEEE, 2000, pp. 1968–1971. ISBN: 978-0-7803-6465-3. DOI: 10.1109/IEMBS.2000.900479.

[37] Daouda Nikiema, Pascale Balland, and Alain Sergent. “Study of the Mechanical Properties of 3D-printed Onyx Parts: Investigation on Printing Parameters and Effect of Humidity”. In: *Chinese Journal of Mechanical Engineering: Additive Manufacturing Frontiers* 2.2 (June 2023), p. 100075. ISSN: 27726657. DOI: 10.1016/j.cjmeam.2023.100075.

[38] Andrej Olenšek et al. “Dynamic balancing responses in unilateral transtibial amputees following outward-directed perturbations during slow treadmill walking differ considerably for amputated and non-amputated side”. In: *Journal of NeuroEngineering and Rehabilitation* 18.1 (July 31, 2021), p. 123. ISSN: 1743-0003. DOI: 10.1186/s12984-021-00914-3.

[39] Miguel Vaca et al. “The Effect of Prosthetic Ankle Dorsiflexion Stiffness on Standing Balance and Gait Biomechanics in Individuals with Unilateral Transtibial Amputation”. In: *JPO Journal of Prosthetics and Orthotics* 36.2 (Apr. 2024), pp. 110–123. ISSN: 1040-8800. DOI: 10.1097/JPO.0000000000000451.

[40] Tyler D. Klenow, Jason T. Kahle, and M. Jason Highsmith. “The dead spot phenomenon in prosthetic gait: Quantified with an analysis of center of pressure progression and its velocity in the sagittal plane”. In: *Clinical Biomechanics* 38 (Oct. 2016), pp. 56–62. ISSN: 02680033. DOI: 10.1016/j.clinbiomech.2016.08.013.